J. metamorphic Geol., 2006, **24,** 153–168 doi:10.1111/j.1525-1314.2006.00631.x

Steady-diffusion modelling of a reaction zone between a metamorphosed basic dyke and a marble from Hirao-dai, Fukuoka, Japan

M. FUKUYAMA[1,2], T. NISHIYAMA[3], K. URATA[4] AND Y. MORI[5]
[1]*National Institute of Advanced Industrial Science and Technology (AIST), Site 7, 1-1-1 Higashi, Tsukuba 305-8567, Japan (m-fukuyama@aist.go.jp)*
[2]*Graduate School of Science and Technology, Kumamoto University, 2-39-1 Kurokami, Kumamoto 860-8555, Japan*
[3]*Department of Earth Science, Kumamoto University, 2-39-1 Kurokami, Kumamoto 860-8555, Japan*
[4]*Department of Geography, Tokyo Metropolitan University, 1-1 Minami-Osawa, Hachioji, Tokyo 192-0397, Japan*
[5]*Kitakyushu Museum of Natural History and Human History, 2-4-1, Higashida, Yahatahigashi-ku, Kitakyushu 805-0071, Japan*

ABSTRACT A reaction zone between a metamorphosed basic dyke and marble at Hirao-dai, north Kyushu, Japan, consists of well-organized sequential zones of diopside, garnet and wollastonite; textures are characteristic of diffusion-controlled structures. The reaction zone formed during contact metamorphism associated with intrusion of a Cretaceous granodiorite at ~300 MPa and 700 °C. The metamorphosed basic dyke consists of diopside, biotite and plagioclase ($X_{Ab} = 0.4$–0.8), whereas the marble is almost pure calcite. The initial boundary between the dyke and the marble is probably located within the current diopside zone, as calcite occurs as remnants among diopside grains in areas close to the boundary with the garnet zone. This observation provides a criterion to judge the stability of the zonal sequence in our modelling. The formation of the reaction zone is attributed to a single-stage steady-state process with five overstepping reactions. CaO, MgO, FeO, SiO_2 and $AlO_{3/2}$ are the reaction-controlling components that are necessary to describe the growth of the reaction zone. An isochemical steady-diffusion model cannot reproduce the measured phase ratios of product minerals; this indicates open-system behaviour of the reaction zone. The choice of closure components is an essential task in the treatment of open-system modelling, together with determination of phase ratios (Ashworth & Birdi model) or estimation of boundary fluxes (Johnson & Carlson model). Of all the possible combinations of closure components, closure conditions for CaO and MgO provide the best results for both models. The stability of the zonal sequence is limited at relatively large values of L_{SiSi}/L_{CaCa}. Similar results from the two models confirm their consistency under the same closure conditions.

Key words: contact metamorphism; open system; reaction zone; steady-diffusion model.

INTRODUCTION

Diffusion-controlled structures in rocks provide valuable information concerning diffusion and reaction kinetics that can be used to interpret the duration and nature of metamorphism (e.g. Fisher, 1978). A reaction zone is a typical diffusion-controlled structure, consisting of a zone or multiple parallel zones. Each zone is a polycrystalline aggregate consisting of one or several mineral species. The major concerns about the growth of a reaction zone are: (i) to understand the mass-balance relationship that controls the growth of a reaction zone; and (ii) to clarify the *L*-ratios that control the stability of the zonal sequence (ratios of proper phenomenological coefficients, viz. L_{ii}/L_{jj}).

Korzhinskii (1959) developed a method, using a chemical potential diagram, in which the occurrence of an observed zonal sequence can be geometrically explained by specifying the diffusion path within the diagram. Although this method is simple and powerful (Brady, 1977; Grant, 1977), it does not explain why nature selects a specific diffusion path from the many possible diffusion paths. The steady-diffusion model formulated by Fisher (1973) and Joesten (1977) is the current standard model; it describes the growth of a reaction zone in terms of an exchange cycle and explains the stability of a zonal sequence in terms of *L*-ratios. This model is a quantitative description of a diffusion path in a chemical potential diagram. The steady-diffusion model has previously been applied to reaction zones (e.g. Nishiyama, 1983; Joesten, 1986a,b, 1991; Joesten & Fisher, 1988).

Several authors have revised and extended the steady-diffusion model. Foster (1981, 1983, 1986) extended the steady-diffusion model to interpret mass transfer between various segregation textures in pelitic rocks. Grant (1988) incorporated some (but not all) cross phenomenological coefficients into the steady-diffusion

model to explain the uphill Ca-diffusion that is necessary to produce observed symplectite proportions and amounts of amphibole in olivine–plagioclase coronas from the western Grenville Province, Canada. Grant's controversial treatment lacks generality, as only L_{CaFe} and L_{CaMg} are considered in the NFCMAS system.

Johnson & Carlson (1990) and Ashworth & Birdi (1990) extended the steady-diffusion model to an open-system environment. On the basis of mass-balance considerations for olivine–plagioclase coronas from the Adirondacks, Johnson & Carlson (1990) demonstrated that net export of Fe, Mg and Na, and net import of Si and Ca occurred during formation of the coronas. The authors introduced boundary-flux equations to describe the flux of components across the outer boundaries of the reaction zone.

Ashworth & Birdi (1990) also demonstrated open-system behaviour for most coronas described in the literature by devising an isocon diagram (Grant, 1986) for symplectites and reactant plagioclase. Ashworth & Birdi (1990) demonstrated that Al and Si are almost conserved in one part of the system, but that other components are not; this observation led them to conclude that Al and Si are conserved in the corona-forming reaction as a whole. To evaluate the open-system behaviour, the authors used the measured overall proportions of the product phase p_m relative to one product phase R, giving 'phase-ratio equations'. Ashworth & Sheplev (1997) subsequently devised a new diffusion model with consideration of affinity, which constrains the absolute values of phenomenological coefficients; this method was subsequently applied to coronal reactions (Ashworth *et al.*, 1998). Attoh (1998) studied various coronas to test the steady-diffusion models of Joesten (1977) and Johnson & Carlson (1990) and concluded that the models are consistent with each other.

Thus the analysis of reaction zones requires a specific interpretation for the reaction zone of interest, and petrologists need to accumulate information from many different case studies to develop a general methodology for interpreting the growth of reaction zones. This paper deals with a reaction zone between a metamorphosed basic dyke and a marble from Hiraodai, Fukuoka, Japan. The reaction zone formed during contact metamorphism related to intrusion of a Cretaceous granodiorite, and consists of three mineral zones: a diopside zone, a garnet zone and a wollastonite zone. In this study, we compare and discuss the results of two versions of the steady-diffusion model in an open system.

REACTION ZONE IN THE HIRAO LIMESTONE

Geological setting

The Hirao Limestone occurs in the Hirao-dai area, north-east of Fukuoka Prefecture, Japan (Fig. 1). The Hirao Limestone is bordered on the north by unmetamorphosed Palaeozoic sandstone and shale of the Kagumeyoshi Formation, with subordinate chert, conglomerate, siliceous shale, greenstone and limestone. The contact between the Kagumeyoshi Formation and the Hirao Limestone is marked by chert mingled with limestone. The Hirao Limestone is bordered on the south by the Tagawa metamorphic rocks, part of the Sangun Metamorphic Rocks of the 230–160 Ma Suo Belt (Nishimura, 1998). The Tagawa

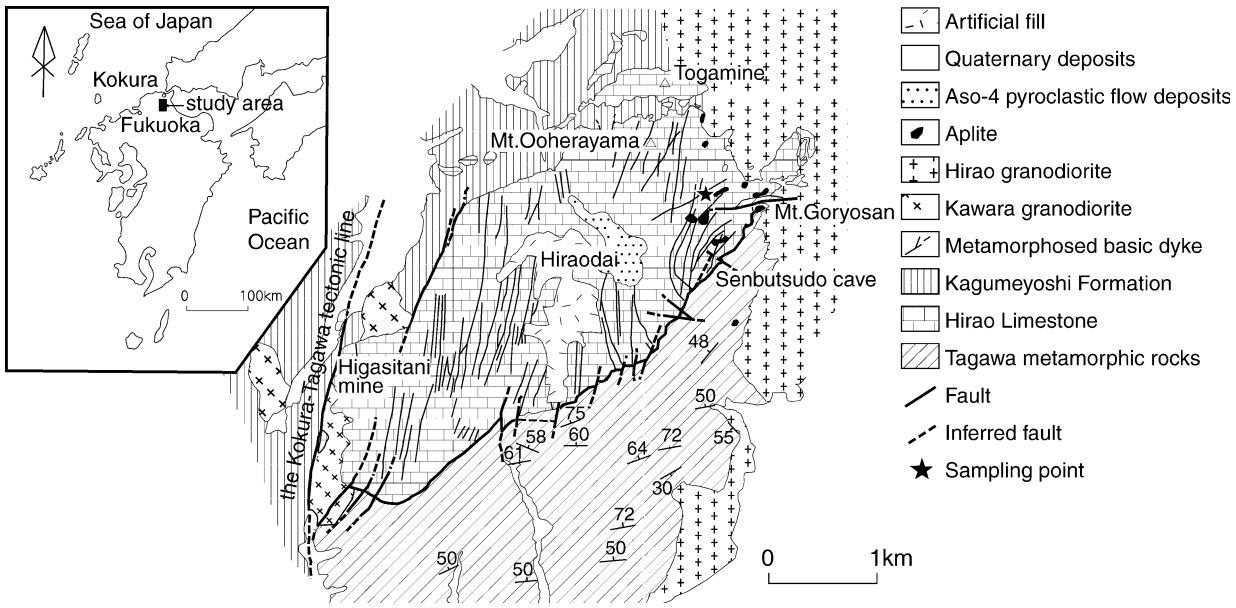

Fig. 1. Geological map of the study area, Hirao-dai, Fukuoka, Japan (after Fukuyama *et al.*, 2004). Star indicates sample locality.

metamorphic rocks consist mainly of pelitic schist with minor basic schist, siliceous schist and calcareous schist. The contact between the Hirao Limestone and the Tagawa metamorphic rocks is either a concordant relationship or a fault. Details of the geological relationships between these units are discussed by Fukuyama *et al.* (2004).

The three geological units described above were intruded by the Hirao granodiorite (K-Ar biotite age of 94 Ma; Kawano & Ueda, 1966) in the eastern Hirao-dai area and underwent extensive contact metamorphism. The metamorphosed Hirao Limestone is an almost pure calcite marble. Skarn minerals (grossular, vesuvianite, wollastonite and others) and ore deposits occur at several places within the contact aureole of the Hirao granodiorite. The size of calcite crystals increases towards the Hirao granodiorite, and reaches a maximum size of several centimetres. The peak physical conditions of the contact metamorphism are estimated to be about 700 °C and 300 MPa (Fukuyama *et al.*, 2004). The conditions of the reaction zone formation are similar to the peak metamorphic conditions, as the sample locality of the reaction zone is close to the contact with the Hirao granodiorite (Fig. 1).

A large number of basic dykes intrude the Hirao Limestone; the dykes are several centimetres to several metres in width and several kilometres in length. The dykes have also been subject to contact metamorphism related to the intrusion of the Hirao granodiorite.

Metamorphosed basic dykes

Reactions between the metamorphosed basic dykes and limestone during contact metamorphism led to the development of reaction zones between the two rock types. In this study, we examine samples of a metamorphosed basic dyke (MB) and associated reaction zones collected at Chagatoko, north-east of Hirao-dai (Fig. 1). The reaction zones consist of three zones, passing from the MB to a diopside zone, garnet zone, wollastonite zone and finally marble (Fig. 2). All zone boundaries are sharp.

Nishiyama (1989) reported a composite vein derived from these reaction zones by hydrofracturing and mass transfer along the fracture. The composite vein consists

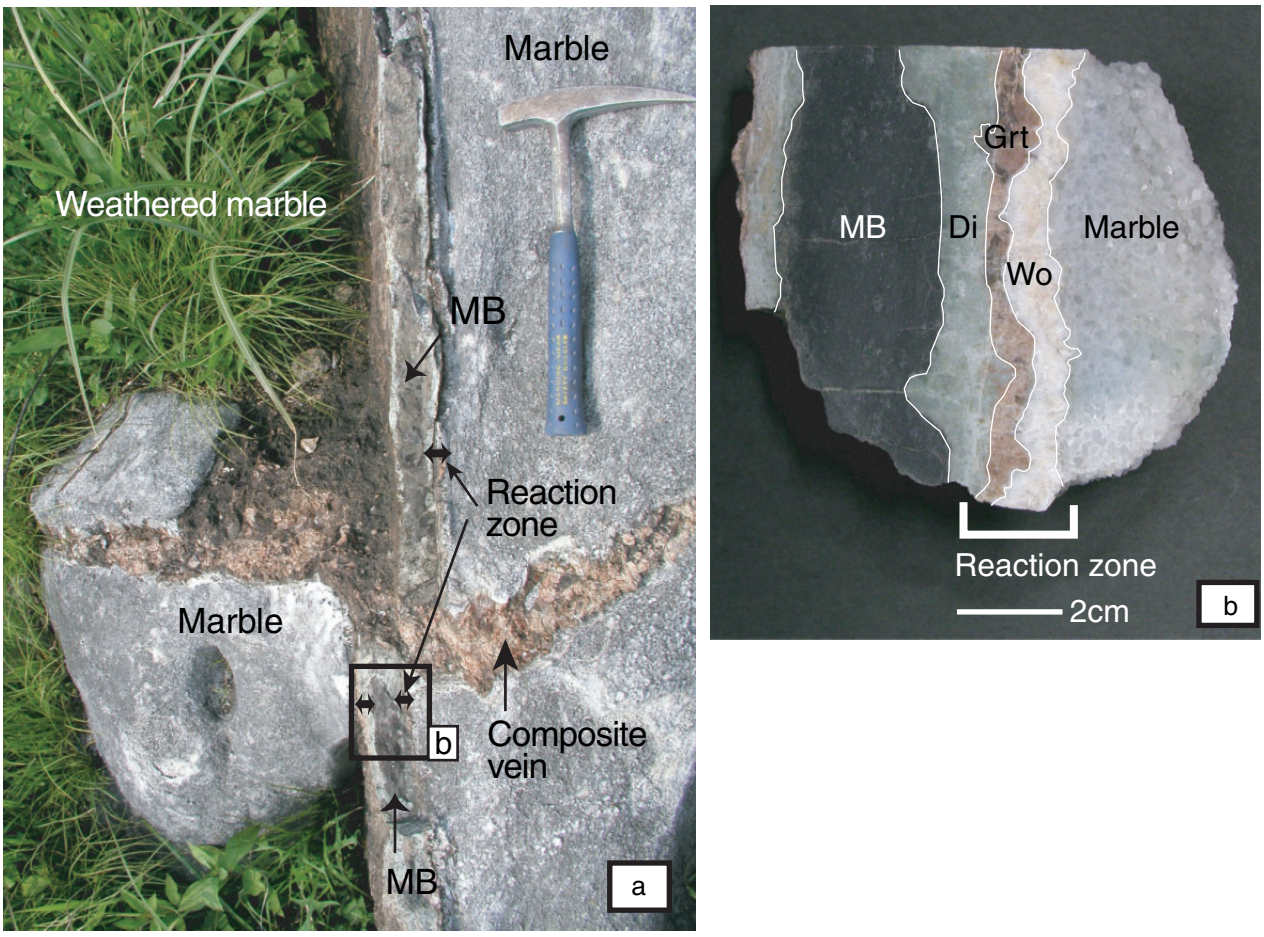

Fig. 2. Photograph showing the outcrop of the reaction zone. Product zones are the diopside zone, garnet zone, and wollastonite zone in this order from the metamorphosed basic dyke to the marble. (a) Marble has been eroded away from the left side of the dyke.

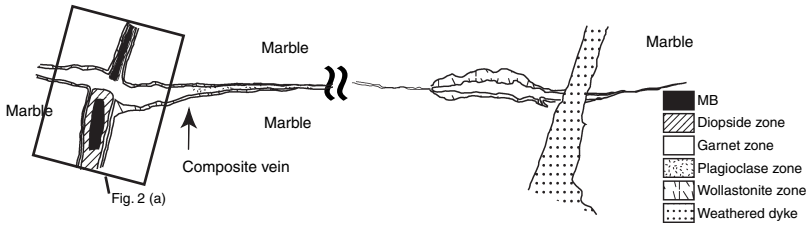

Fig. 3. Sketch of the outcrop photographed in Fig. 2a. The composite vein is derived from the reaction zone between the metamorphosed basic dyke (MB) and the marble.

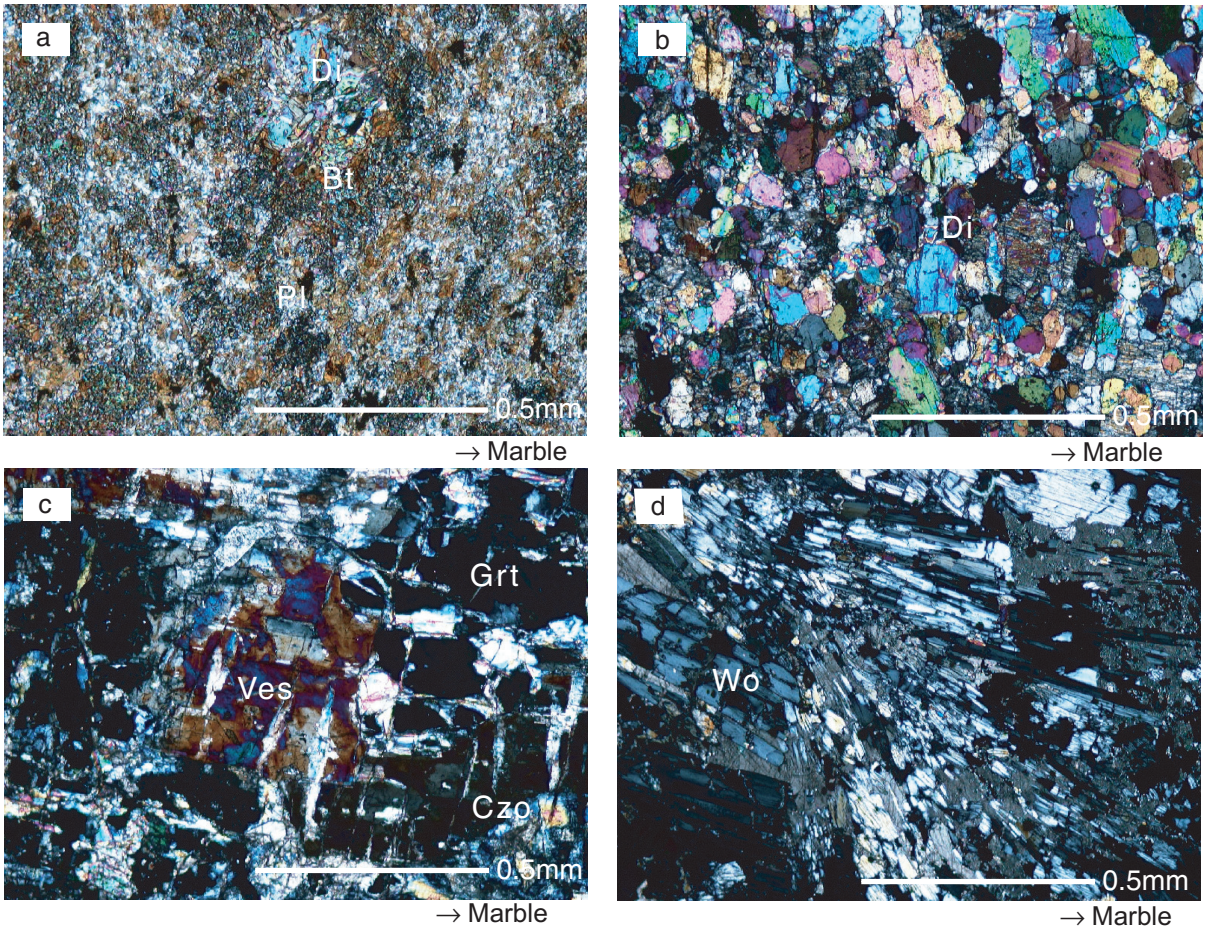

Fig. 4. Photomicrographs of representative samples. (a) Metamorphosed basic dyke consisting of biotite + plagioclase + diopside. (b) Diopside zone adjacent to the metamorphosed basic dyke, consisting mainly of diopside. (c) Garnet zone consisting of garnet + clinozoisite + vesuvianite. (d) Wollastonite zone adjacent to the marble, consisting of wollastonite. The plate shows the growth direction of wollastonite from the garnet zone to the marble. Mineral abbreviations here and throughout the paper are after Kretz (1983).

of garnet, plagioclase and wollastonite. The vein is dominantly composed of garnet near the reaction zones and dominantly plagioclase at a distance of 2 m from the reaction zones (Fig. 3).

Petrography

Metamorphosed basic dyke

The metamorphosed basic dyke is dark brown and massive, consisting mainly of biotite, diopside and plagioclase with minor pyrrhotite, titanite, apatite and K-feldspar. Chlorite occurs as a secondary mineral along the boundary between the MB and the diopside zone, whereas chalcopyrite and spinel occur as accessory minerals (Fig. 4a). The MB is completely recrystallized, with sporadic diopside aggregates up to 3 mm in diameter within a matrix of biotite, diopside and plagioclase. No preferred orientation of minerals is observed. Diopside occurs in the matrix as short anhedral to subhedral prismatic crystals 0.07 mm in length. Diopside within aggregates is much coarser, up

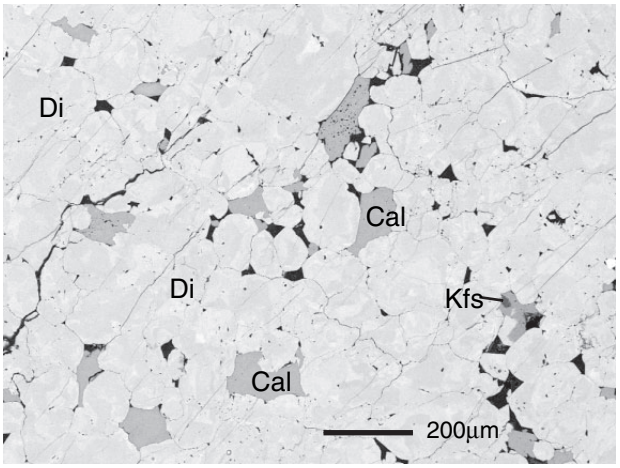

Fig. 5. Backscattered electron image of the diopside zone showing residual calcite interstitial to diopside grains.

to 0.4 mm in length. Biotite occurs as anhedral to subhedral tabular crystals ranging from 0.9 to 2 mm in size. Plagioclase occurs as subhedral crystals up to 0.1 mm in size, whereas K-feldspar occurs as fine-grained anhedral crystals 0.01 mm in size. Apatite occurs as fine-grained anhedral crystals 0.1 mm in size. Titanite occurs in biotite along cleavage planes or within crystal rims, and occurs at the boundaries between minerals.

Diopside zone

The diopside zone is bluish-green with a width of 1–2 cm, and consists mainly of diopside with minor plagioclase, titanite and apatite (Fig. 4b). Calcite occurs within the interstices of diopside grains within a zone (8.41 mm wide) adjacent to the diopside–garnet zone boundary (Fig. 5). Rare analcite and orthoclase occupy the interstices between diopside grains in other parts of the zone. These observations indicate that the initial boundary between the MB and the marble was located in the current diopside zone. Diopside occurs as anhedral crystals 0.15–0.3 mm in size, and is finer-grained near the boundary with the garnet zone. Apatite occurs as fine-grained anhedral crystals 0.1 mm in size. Titanite occurs along the boundaries between minerals.

Garnet zone

The garnet zone is 0.2–1.1 cm wide, and composed mainly of garnet, vesuvianite, clinozoisite and minor diopside, plagioclase, titanite and apatite (Fig. 4c). Garnet occurs as fine-grained aggregates of irregular shape. Vesuvianite occurs as large crystals ~5 mm in size, with oscillatory zoning. Clinozoisite forms a network vein in the garnet zone, indicating a secondary origin. Apatite occurs as short anhedral to subhedral columnar crystals 0.1–1 mm in size. Titanite occurs within garnet along cleavage planes.

Wollastonite zone

The wollastonite zone is 0.2–0.8 cm wide, and is made up almost entirely of wollastonite with rare plagioclase and diopside. Radial aggregates of wollastonite show a growth direction towards the marble (Fig. 4d). Wollastonite is occasionally replaced by secondary quartz and calcite.

Modal compositions within the reaction zone

Each of the mineral zones consists dominantly of just one mineral species or a small number of species (Fig. 6). The modal composition of the metamorphosed basic dyke is biotite 50%, diopside 33%, plagioclase 16% and others 1% (titanite, pyrrhotite, apatite, K-feldspar, chlorite, chalcopyrite and spinel). The model composition of the diopside zone is diopside 91%, plagioclase 6% and others 3% (titanite, apatite, chlorite and chalcopyrite and spinel). The garnet zone is garnet 67%, clinozoisite 17%, plagioclase 7%, diopside 4%, vesuvianite 3% and others 2% (titanite, apatite and K-feldspar), whereas the wollastonite zone consists of wollastonite 93% and others 7% (diopside, garnet, plagioclase, calcite and quartz).

Bulk composition of the reaction zone

Representative bulk-rock compositions of the mineral zones, MB and marble are listed in Table 1. The compositions represent an average of three measurements. The relative standard deviations indicate 1σ of the measurements. Whole-rock compositions were analysed using a PANalytical MagiX Pro housed at the Kitakyushu Museum of Natural History and Human History, Japan. Sample preparation and analytical procedures follow Mori & Mashima (2005), except for marble samples, for which we follow Goto *et al.* (2002). A Perkin-Elmer 2400 II CHN analyser was used for determining H_2O and CO_2 contents.

Mineral chemistry

Quantitative chemical analyses of minerals were performed with an energy-dispersive X-ray microanalyzer JEOL PC-SEM 5600 combined with a LINK ISIS system, housed at Kumamoto University, Japan. The accelerating voltage was 20 kV, and electron-beam current was set to 0.6 nA. Representative analyses of minerals are shown in Table 2.

Biotite

Biotite has an almost constant composition of X_{Mg} (Mg/Fe + Mg) = 0.71–0.77 throughout the MB,

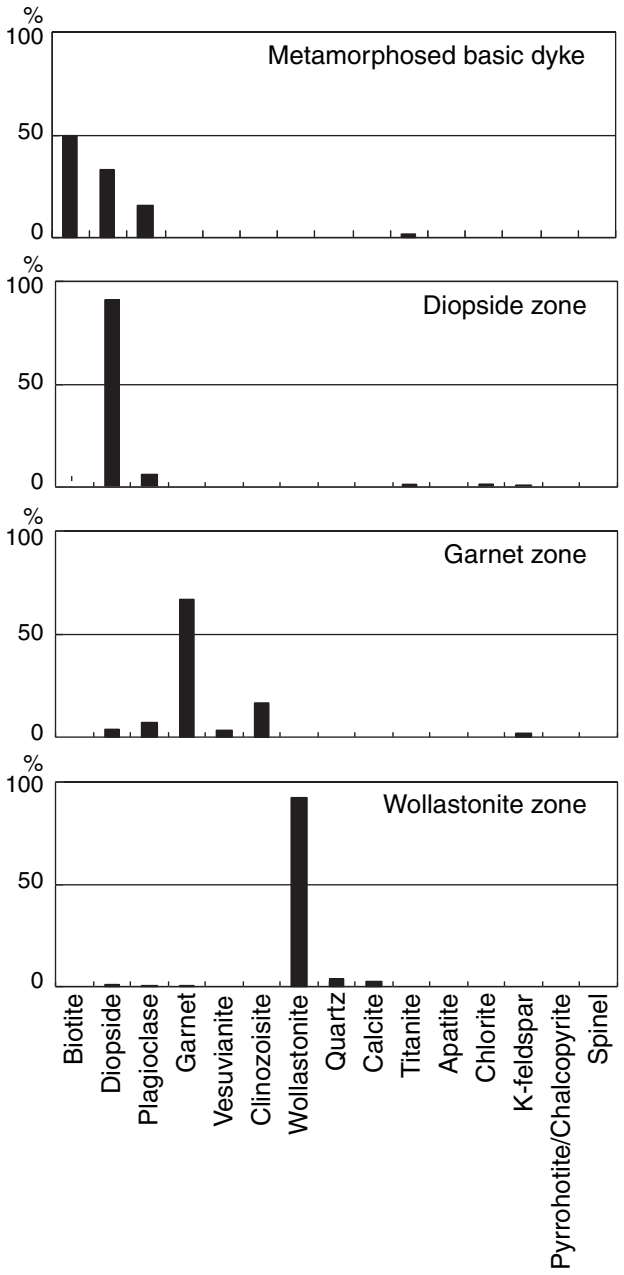

Fig. 6. Modal compositions of the metamorphosed basic dyke and mineral zones.

irrespective of the distance from the contact with the diopside zone (Fig. 7).

Diopside

Diopside occurs both in the diopside zone and in the MB. Diopside in the MB has $X_{Mg} = 0.74$–0.83, whereas diopside in the diopside zone is more iron-rich ($X_{Mg} = 0.56$–0.86; Fig. 7). No systematic compositional variation was observed with distance from the contact between the MB and the diopside zone.

Plagioclase

Plagioclase shows a large compositional variation from $X_{Ab} = 0.4$–0.8 within the MB, and from $X_{Ab} = 0.4$–1.0 in the diopside zone (Fig. 7).

Garnet

The composition of garnet within the garnet zone is $Grs_{82-97}Adr_{3-11}Alm_{0-5}Sps_{0-2}$.

MODELLING OF THE REACTION ZONE

The reaction zone analysed in this study is typical of those formed by the interplay of reaction and diffusion through an intergranular medium. The process of formation of the reaction zone can be summarized as follows. Originally, the basic dyke was in contact with the limestone. During contact metamorphism associated with intrusion of the Hirao Granodiorite, reactions took place between the dyke and limestone, forming zones of product minerals across which diffusion of several components was driven by chemical potential gradients. MgO, FeO, $AlO_{3/2}$ and SiO_2 components were released from the MB and moved towards the marble, whereas a CaO component moved from the marble towards the MB. The lack of $KO_{1/2}$- or $NaO_{1/2}$-bearing minerals in the reaction zone requires an open-system description of reaction zone formation. An isocon analysis (Gresens, 1967; Grant, 1986: Baumgartner & Olsen, 1995) was tried first as a means of determining the inert components and the amounts of mobile components gained or lost. Isocon diagrams were constructed for the diopside zone taking the MB as a protolith, and for the diopside, garnet and wollastonite zones taking the marble as a protolith, as the initial dyke–limestone contact is located within the current diopside zone. Unfortunately, it was not possible to define an isocon in these diagrams, as the distribution of data is too scattered. An alternative approach is therefore required to describe the formation of the reaction zone.

The sharp boundaries between adjacent mineral zones indicate diffusion-controlled growth of the reaction zone. Under such a condition, the system is in local equilibrium (Thompson, 1959), and diffusion of a chemical component is driven by its chemical potential gradient. There is no compositional variation within individual mineral species in each mineral zone (Fig. 7), which is consistent with the assumption that the reaction zone is a diffusion-controlled structure in which the mineral assemblage and mineral compositions did not change during the formation of the reaction zone. The reaction zone is therefore suitable for analysis via a steady-diffusion model. In this analysis, two versions of the steady-diffusion model (Ashworth & Birdi, 1990; Johnson & Carlson, 1990) were used; both are open-system models.

Table 1. Whole-rock compositions and densities of the reaction zone.

Lithology	MB (1σ)	Di zone (1σ)	Grt zone (1σ)	Wo zone (1σ)	Marble (1σ)
(wt%)					
SiO_2	49.62 (0.21)	49.62 (0.01)	38.47 (0.01)	44.55 (0.04)	n.d.
TiO_2	0.64 (0.00)	0.20 (0.00)	0.62 (0.00)	0.01 (0.00)	0.03 (0.00)
Al_2O_3	14.16 (0.06)	3.86 (0.01)	17.88 (0.02)	0.30 (0.00)	0.03 (0.00)
$Fe_2O_3^a$	7.42 (0.04)	8.80 (0.01)	4.81 (0.01)	0.59 (0.00)	0.04 (0.00)
MnO	0.13 (0.00)	0.39 (0.00)	0.44 (0.00)	0.14 (0.00)	0.01 (0.00)
MgO	10.67 (0.02)	10.22 (0.00)	0.82 (0.00)	0.78 (0.00)	0.67 (0.00)
CaO	10.07 (0.07)	25.91 (0.01)	32.87 (0.04)	43.64 (0.04)	54.55 (0.06)
Na_2O	2.37 (0.00)	0.22 (0.00)	0.44 (0.00)	0.09 (0.00)	n.d.
K_2O	3.64 (0.03)	0.06 (0.00)	0.05 (0.00)	n.d.	n.d.
P_2O_5	0.19 (0.00)	0.11 (0.00)	0.04 (0.00)	0.01 (0.00)	0.02 (0.00)
H_2O	1.10 (0.04)	0.15 (0.04)	0.45 (0.00)	0.18 (0.00)	n.d.
CO_2	0.06 (0.02)	0.65 (0.02)	1.54 (0.00)	8.37 (0.02)	43.78 (0.09)
Total	100.09	100.20	98.44	98.66	99.12
(ppm)					
Sc	26 (1)	22 (0)	n.d.	n.d.	n.d.
V	159 (1)	77 (1)	92 (2)	n.d.	n.d.
Cr	785 (4)	613 (1)	n.d.	n.d.	n.d.
Ni	300 (3)	207 (1)	17 (1)	n.d.	n.d.
Cu	42 (1)	n.d.	n.d.	n.d.	n.d.
Zn	297 (1)	421 (3)	71 (1)	20 (0)	n.d.
Rb	761 (3)	15 (2)	5 (2)	n.d.	n.d.
Sr	1030 (4)	56 (1)	103 (1)	54 (1)	233 (0)
Y	13 (0)	15 (1)	31 (1)	9 (1)	12 (1)
Zr	79 (1)	76 (1)	35 (0)	7 (1)	14 (1)
Nb	6 (0)	28 (0)	74 (0)	n.d.	n.d.
Ba	529 (9)	32 (5)	18 (4)	n.d.	21 (14)
La	n.d.	n.d.	n.d.	n.d.	n.d.
Ce	n.d.	n.d.	21 (1)	n.d.	n.d.
Nd	n.d.	n.d.	n.d.	n.d.	n.d.
Pb	11 (1)	n.d.	n.d.	n.d.	20 (5)
Density (g cm^{-3})	2.96	3.24	3.51	2.77	2.69

[a]Total iron as Fe_2O_3.
n.d. = not detected.

Table 2. Representative analyses of minerals in the reaction zone.

Zone	Metamorphosed basic dyke			Diopside zone	Garnet zone	Wollastonite zone
Mineral	Biotite	Diopside	Plagioclase	Diopside	Grossular	Wollastonite
SiO_2	40.28	54.29	61.49	54.24	39.17	52.97
Al_2O_3	14.37	0.00	24.65	0.00	20.46	0.00
FeO	11.79	7.33	0.00	6.40	2.85	0.00
MgO	17.59	14.04	0.00	14.86	0.00	0.00
MnO	0.00	0.00	0.00	0.00	0.00	0.00
TiO_2	1.62	0.00	0.00	0.00	1.27	0.00
CaO	0.00	24.41	5.68	24.64	36.27	48.02
Na_2O	0.00	0.00	8.31	0.00	0.00	0.00
K_2O	10.94	0.00	0.00	0.00	0.00	0.00
Total	96.59	100.07	100.13	100.14	100.02	100.99
Oxygen	22	6	8	6	12	3
Si	5.85	2.01	2.72	2.00	2.98	1.01
Al	2.46	0.00	1.29	0.00	1.84	0.00
Fe	1.43	0.23	0.00	0.20	0.18	0.00
Mg	3.81	0.78	0.00	0.82	0.00	0.00
Mn	0.00	0.00	0.00	0.00	0.00	0.00
Ti	0.18	0.00	0.00	0.00	0.07	0.00
Ca	0.00	0.97	0.27	0.98	2.96	0.98
Na	0.00	0.00	0.71	0.00	0.00	0.00
K	2.03	0.00	0.00	0.00	0.00	0.00
Total	15.76	3.99	4.99	4.00	8.03	1.99

Steady-diffusion model

The steady-diffusion model is based on the principle of linear irreversible thermodynamics (e.g. Katchalsky & Curran, 1965; Prigogine, 1967; de Groot & Mazur, 1984). It assumes that departures from equilibrium are so small that linear phenomenological equations hold between thermodynamic forces and fluxes. In the linear regime of a non-equilibrium state, the system will reach a state of minimum rate of entropy production, which is equivalent to a steady state. Fisher (1973) was the first to develop irreversible thermodynamic formulations for diffusion through an intergranular medium during metamorphism. He found that a ratio of diffusive fluxes can be simply expressed by a ratio of stoichiometric coefficients at steady state, which provides a firm basis for the steady-diffusion model. Joesten (1977) further developed the steady-diffusion equation in terms of a reaction zone, and presented a framework to describe the growth of a reaction zone in terms of an exchange cycle. He also showed that the stability of a zonal sequence in a reaction zone depends on *L*-ratios (ratios of phenomenological coefficients). The following is a brief summary of the steady-diffusion model of a closed system as proposed by Fisher (1973) and Joesten (1977), which forms the basis of the open-system model.

Consider a system at constant pressure and temperature that consists of several mineral zones between two reactants. The zones are bounded on either side by sharp contacts (the zone boundary). It is assumed that the grain boundaries are filled with an intergranular

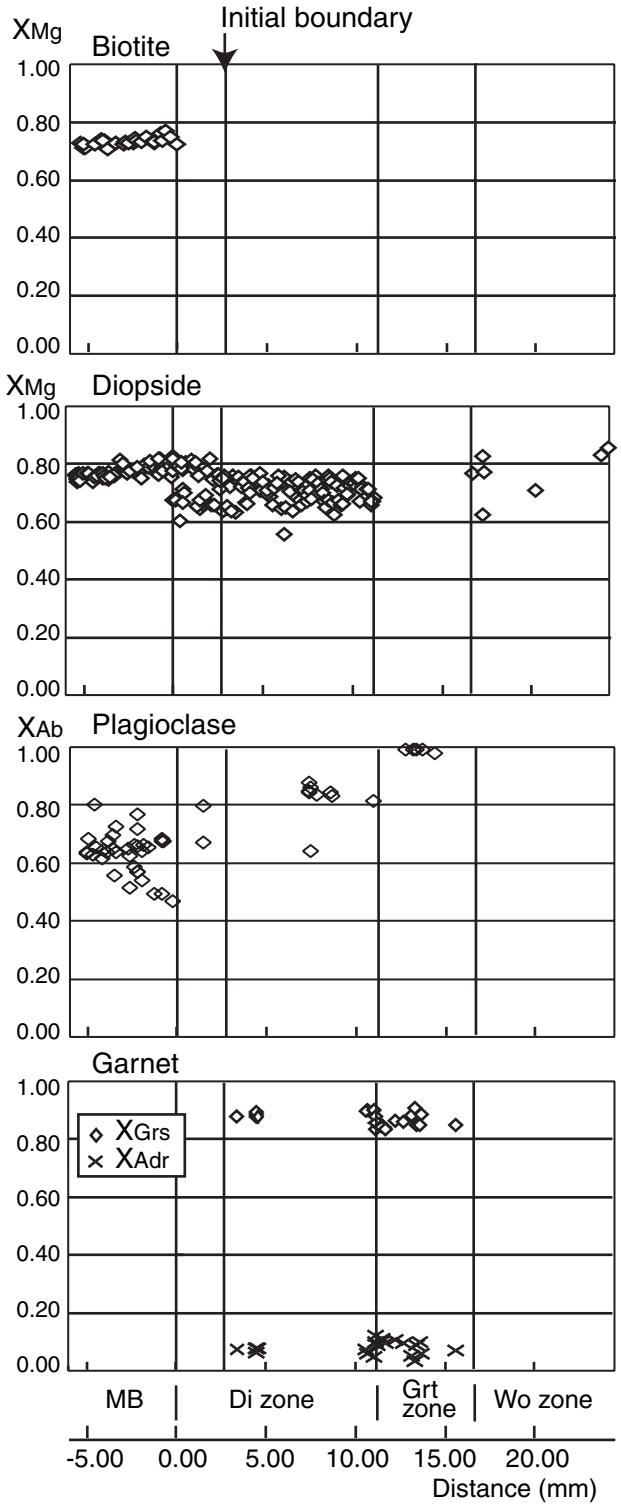

Fig. 7. Mineral compositions of biotite, diopside, plagioclase and garnet, plotted against distance from the boundary between the metamorphosed basic dyke and the diopside zone.

fluid and that chemical components produced by reactions at the zone boundaries diffuse down chemical potential gradients through the fluid and across the zones. If the growth rate of the zones is sufficiently small, diffusion through the intergranular fluid can be described within a reference frame fixed with respect to the zone boundary. The model requires the following assumptions: (i) the diffusing components in the intergranular fluid are everywhere in local equilibrium with adjacent solids; (ii) chemical reactions occur only at the zone boundaries and no reactions take place within the mineral zones; and (iii) diffusion is limited within the mineral zones and diffusion of the reactant phases is negligible. Based on these assumptions, the one-dimensional steady-diffusion model consists of four kinds of equations, as described below.

Mass-balance equations in zone boundary reactions

The mass-balance equation for the diffusing component i in a zone boundary reaction, which relates the amount of each component consumed or produced at the zone boundary to the amount of each phase involved in the reaction at the zone boundary, can be written as:

$$v_i^{X-YZ} = \sum v_\phi^{X-YZ} n_i^\phi,$$

where v_i^{X-YZ} is the number of moles of component i consumed or produced in the zone boundary between mineral phases X and $Y + Z$, v_ϕ^{X-YZ} is the stoichiometric coefficient of phase ϕ involved in the zone boundary reaction, and n_i^ϕ is the formula proportion of component i in phase ϕ. A mass-balance equation is required for each diffusing component in the zone boundary reaction.

Steady-diffusion equations

The steady-state condition means that the concentration of component i in a local volume is independent of time, irrespective of the existence of a diffusive flux of i, J_i. The diffusive flux can be written as

$$J_i = \sum_{i=1}^{n_c} -L_{ij} \frac{\mathrm{d}\mu_i}{\mathrm{d}x},$$

where L_{ij} is the phenomenological coefficient that relates the flux J_i to the chemical potential gradient $\mathrm{d}\mu_i/\mathrm{d}x$ for each of the n_c diffusive components.

No reactions take place within the mineral zones, resulting in a constant diffusive flux everywhere, that is $J_i =$ constant. At a zone boundary, a source term (the number of moles of component i consumed or produced due to chemical reaction at the zone boundary) must balance the difference between inflow and outflow of diffusive flux

$$v_i^{X-YZ} = J_i^{YZ(\mathrm{out})} - J_i^{X(\mathrm{in})},$$

where $J_i^{YZ(\mathrm{out})}$ is the diffusive flux of component i in zone $Y + Z$ lying on the lower-potential side of the zone boundary $X - YZ$, $J_i^{X(\mathrm{in})}$ is the diffusive flux of

the same component in zone X, which lies on the higher-potential side of the boundary, and v_i^{X-YZ} is the number of moles of component i consumed or produced in the zone boundary between mineral phases X and $Y + Z$.

Flux-ratio equations

The flux-ratio equation comes from the Gibbs–Duhem relationship(s) for a mineral or a mineral assemblage that makes up a zone through which diffusion takes place. The requirement of local equilibrium between diffusing components and adjacent minerals provides a condition that diffusive fluxes should satisfy the Gibbs–Duhem relationship for the mineral. The Gibbs–Duhem equation for a two-component mineral at constant pressure and temperature is

$$n_i^{\phi}\,\mathrm{d}\mu_i^{\phi} + n_j^{\phi}\,\mathrm{d}\mu_j^{\phi} = 0,$$

where μ_i^{ϕ} and μ_j^{ϕ} are the chemical potentials of components i and j in phase ϕ respectively. The diffusive fluxes for components i and j within layer X can be written as

$$J_i^X = -L_{ii}\left(\frac{\mathrm{d}\mu_i}{\mathrm{d}x}\right), \quad J_j^X = -L_{jj}\left(\frac{\mathrm{d}\mu_j}{\mathrm{d}x}\right)$$

By combining these equations, we have

$$\frac{n_i^{\phi} J_i^X}{n_j^{\phi} J_j^X} = -\frac{L_{ii}}{L_{jj}}$$

Thus the flux-ratio equation implies a dependence between diffusive fluxes because of the local equilibrium requirement, which is given by the ratio of phenomenological coefficients. In this treatment, cross terms in the phenomenological equations are neglected ($L_{ij} = 0$ for $i \neq j$).

Extent-of-reaction equation

The extent of the reaction must be specified by the following equation:

$$v_i^{X-YZ} = \xi,$$

where ξ is a non-zero constant specifying the progress of the reaction in terms of the amount of one of the reactants consumed. This equation must be included because the total amount of material involved in transport and reaction must be directly proportional to the total amount of reactants consumed.

Steady-diffusion models in an open system

The closed-system model described above predicts the overall proportions of minerals produced, which is commonly inconsistent with observations from field samples. This inconsistency arises mostly from the open-system behaviour of components that are neglected in the closed-system model. Two versions of a revised model have been proposed to incorporate open-system behaviour. Ashworth & Birdi (1990) proposed a model that employs the ratios of product minerals and assumes that only Al and Si components show closed-system behaviour. Johnson & Carlson (1990) presented a model that describes open-system reactions by estimating the flux across the system's outer zone boundaries.

Phase-ratio equations (Ashworth & Birdi, 1990)

The steady-diffusion equation does not hold for open components. Instead, new constraints, the phase-ratio equations, are introduced to arrive at a solution. The phase-ratio equations give the overall proportions of product phase p_m relative to one product phase R with $p_R = 1$

$$v_m = p_m v_R$$

where molar proportions v_m and v_R are converted from measured volume proportions. The open-system model of Ashworth & Birdi (1990) consists of mass balance equations, flux-ratio equations, steady-diffusion equations for closure components, phase-ratio equations, and extent-of-reaction equations.

Boundary-flux equations (Johnson & Carlson, 1990)

The boundary-flux equations define the diffusive fluxes into or out of the system across the outermost zone boundaries

$$J_i^b = k_i$$

in which J_i^b is the flux of diffusing component i into or out of the reaction zone at either extreme boundary of the reaction zone, and k_i is the amount of component i corresponding to the amount of reaction specified in the extent-of-reaction equations. One boundary-flux equation is required for each diffusing component at each of the two outermost zone boundaries.

RESULTS FOR THE REACTION ZONE AT HIRAO-DAI

Application of the steady-diffusion model

A requirement of both methods outlined above is the need to specify components that exhibit closed-system (or open-system) behaviour. First, we will specify the system in terms of reactant and product phases and reaction-controlling components. Each of the three mineral zones can be approximated as a monomineralic zone; the zonal sequence is therefore as follows: metamorphosed basic dyke (MB)/diopside zone/garnet zone/wollastonite zone/marble (calcite). The MB consists mainly of biotite, plagioclase and diopside. Thus the reactant phases will be biotite, plagioclase, diopside and calcite.

The number of components n_c that exert diffusive control on the reaction can be calculated via the following equation (Johnson & Carlson, 1990):

$$n_c = \sum_{i=1}^{n_i} n_{p,i} - \sum_{l=1}^{n_l} n_{p,l} - n_r$$

where $n_{p,i}$ denotes the number of distinct phases at zone boundary i, $n_{p,l}$ is the number of phases present in zone l, and n_r represents the number of equilibrium boundaries that are overstepped before the reaction begins. n_r can be calculated as follows (Thompson, 1982). The number of model system components (c_s) is nine (Na_2O, K_2O, CaO, MgO, FeO, Al_2O_3, SiO_2, H_2O, CO_2). The number of model phase components (c_p) for phases participating in the overall reaction is 14 [annite, phlogopite, albite, anorthite, diopside, hedenbergite, grossular, almandine, wollastonite, calcite, fluid (CO_2, H_2O, K_2O, Na_2O)]. The number of linearly independent reactions therefore becomes $n_r = c_p - c_s = 5$. Thus we can calculate n_c as follows:

$$n_c = (6 + 4 + 3 + 2) - (2 + 2 + 1) - 5 = 5$$

Therefore CaO, MgO, FeO, $AlO_{3/2}$ and SiO_2 are taken as the components necessary and sufficient to describe the model. Ferric iron will not take part in the reaction because reactant phases are free from ferric iron and only garnet in the garnet zone contains small amounts of ferric iron.

Components with open-system behaviour must also be specified in the two open-system methods. Mineral compositions and phase ratios listed in Table 3 are used in the following discussion. Table 3 shows the idealized stoichiometric formulae of reactant and product minerals, the average widths of each zone, the molar proportions of the MB, and the molar proportions of reaction products. The average width of each zone is used for determining the molar proportions of products. Garnet composition is approximated as grossular–almandine, neglecting the andradite component. We applied both models to the reaction zone, maintaining constant reactant-phase ratios in the MB and the product.

Table 3. Idealized stoichiometric formulas of minerals and measured product proportions.

Zone	Metamorphosed basic dyke			Diopside zone	Garnet zone	Wollastonite zone
Mineral	Biotite	Diopside	Plagioclase	Diopside	Garnet[a]	Wollastonite
Si	5.82	2.00	2.64	2.00	3.00	1.00
Al	2.48	0.00	1.36	0.00	2.00	0.00
Fe	1.42	0.23	0.00	0.28	0.14	0.00
Mg	3.89	0.77	0.00	0.72	0.00	0.00
Mn	0.00	0.00	0.00	0.00	0.00	0.00
Ti	0.16	0.00	0.00	0.00	0.00	0.00
Ca	0.00	1.00	0.36	1.00	2.86	1.00
Na	0.00	0.00	0.64	0.00	0.00	0.00
K	2.00	0.00	0.00	0.00	0.00	0.00
$\sum$	15.77	4.00	5.00	4.00	8.00	2.00
O	22.00	6.00	8.00	6.00	12.00	3.00
Thickness (mm)	2.76[b]			11.17	5.43	7.67
Product proportions (mol.%)	50.39	16.14	33.47	41.55	10.79	47.65

[a]Garnet is approximated to $Ca_{2.86}Fe_{0.14}Al_{2.00}Si_{3.00}O_{12}$.
[b]Thickness from initial boundary in the diopside zone to MB.

Results of the Ashworth & Birdi (1990) model

The Ashworth & Birdi (1990) model requires phase-ratio equations and two closure equations (steady-diffusion equations for closure components). In the case study of Ashworth & Birdi (1990), they imposed the condition that Al and Si components are closed within the reaction zone: they are not transported beyond the outer boundaries of the reaction zone. One candidate for the closure component in our case is CaO, because CaO diffuses from the marble towards the MB (the MB has a small finite volume), and no further transportation of CaO beyond the MB is possible. There are four candidates for the remaining closure component: MgO, FeO, $AlO_{3/2}$ and SiO_2. The four different possible combinations yield the following overall reactions.

Case 1. CaO and MgO are the closure components:

$$\begin{aligned} &0.07K_{2.00}Mg_{3.89}Fe_{1.42}Al_{2.48}Ti_{0.16}Si_{5.82}O_{20}(OH)_4 \\ &\quad + 0.02Na_{0.64}Ca_{0.36}Al_{1.36}Si_{2.64}O_8 \\ &\quad + 0.05CaMg_{0.77}Fe_{0.23}Si_{2.00}O_6 \\ &\quad + 1.15CaCO_3 + 1.09SiO_2 \\ &\quad + 0.03FeO + 0.02AlO_{3/2} \\ &\quad = 0.42CaMg_{0.72}Fe_{0.28}Si_2O_6 \\ &\quad + 0.11Ca_{2.86}Fe_{0.14}Al_{2.00}Si_{3.00}O_{12} \\ &\quad + 0.48CaSiO_3 + 0.01TiO_2 + 0.01NaO_{1/2} \\ &\quad + 0.14KO_{1/2} + 0.14H_2O + 1.15CO_2 \end{aligned}$$

Case 2. CaO and FeO are the closure components:

$$\begin{aligned} &0.08K_{2.00}Mg_{3.89}Fe_{1.42}Al_{2.48}Ti_{0.16}Si_{5.82}O_{20}(OH)_4 \\ &\quad + 0.03Na_{0.64}Ca_{0.36}Al_{1.36}Si_{2.64}O_8 \\ &\quad + 0.06CaMg_{0.77}Fe_{0.23}Si_{2.00}O_6 + 1.13CaCO_3 \\ &\quad + 0.96SiO_2 = 0.42CaMg_{0.72}Fe_{0.28}Si_{2.00}O_6 \\ &\quad + 0.11Ca_{2.86}Fe_{0.14}Al_{2.00}Si_{3.00}O_{12} + 0.48CaSiO_3 \\ &\quad + 0.07MgO + 0.03AlO_{3/2} + 0.01TiO_2 \\ &\quad + 0.01NaO_{1/2} + 0.17KO_{1/2} + 0.17H_2O + 1.13CO_2 \end{aligned}$$

Case 3. CaO and $AlO_{3/2}$ are the closure components:

$$\begin{aligned} &0.07K_{2.00}Mg_{3.89}Fe_{1.42}Al_{2.48}Ti_{0.16}Si_{5.82}O_{20}(OH)_4 \\ &\quad + 0.02Na_{0.64}Ca_{0.36}Al_{1.36}Si_{2.64}O_8 \\ &\quad + 0.05CaMg_{0.77}Fe_{0.23}Si_2O_6 + 1.14CaCO_3 \\ &\quad + 1.04SiO_2 + 0.02FeO \\ &\quad = 0.42CaMg_{0.72}Fe_{0.28}Si_{2.00}O_6 \\ &\quad + 0.11Ca_{2.86}Fe_{0.14}Al_{2.00}Si_{3.00}O_{12} + 0.48CaSiO_3 \\ &\quad + 0.03MgO + 0.01TiO_2 + 0.01NaO_{1/2} \\ &\quad + 0.15KO_{1/2} + 0.15H_2O + 1.14CO_2 \end{aligned}$$

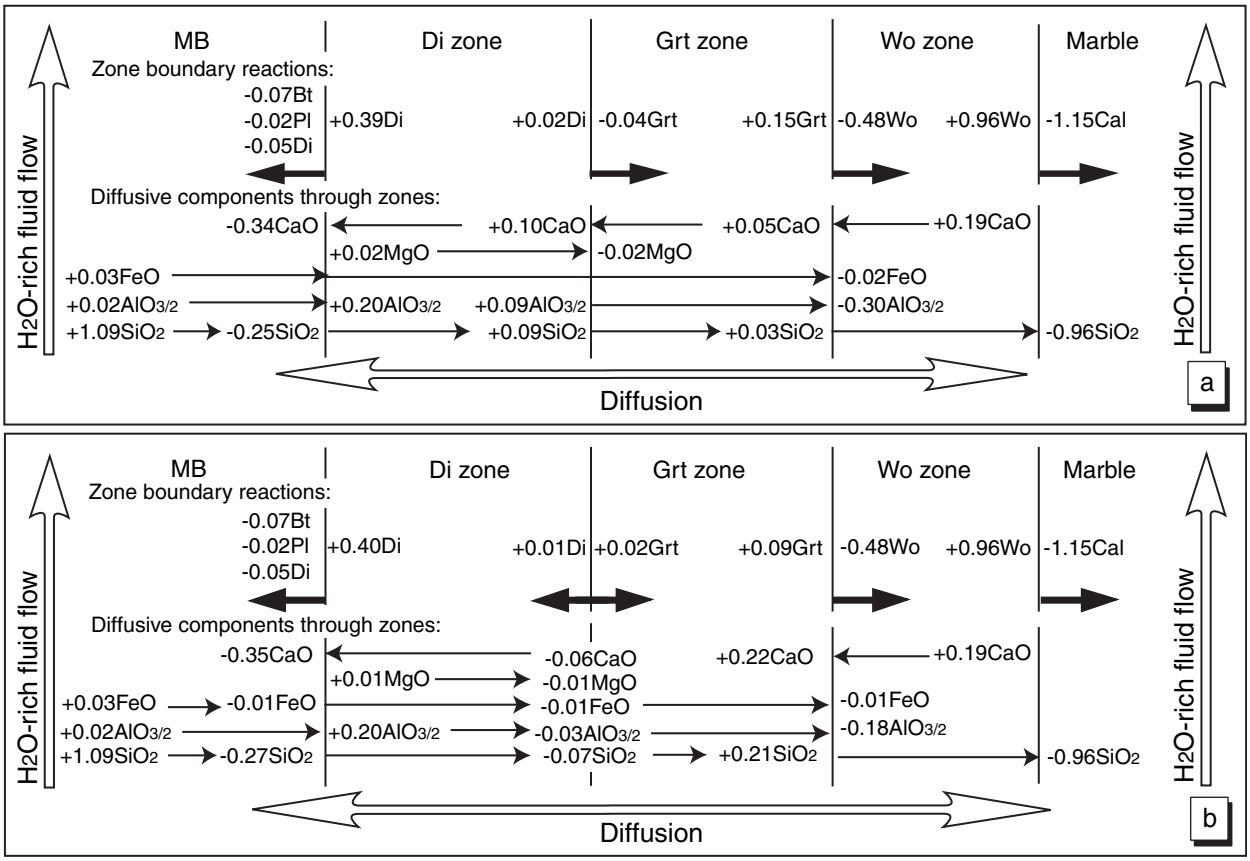

Fig. 8. Example of the exchange cycle of the reaction zone in the steady-diffusion model (Ashworth & Birdi, 1990). (a) An exchange cycle of the reaction zone for $L_{SiSi}/L_{CaCa} = 5$ and $L_{SiSi}/L_{ii} = 1$. (b) Example of an exchange cycle ($L_{SiSi}/L_{CaCa} = 5$ and $L_{SiSi}/L_{ii} = 10$) in which the zonal sequence of the reaction zone is unstable. At the diopside–garnet zone boundary, both minerals are produced, although one of them should be consumed. 'Plus' signs denote the component produced, whereas 'minus' signs denote the component consumed. Thin arrows indicate the direction of movement of components. Bold arrows indicate the growth directions of mineral zones.

Case 4. CaO and SiO_2 are the closure components:

$$\begin{aligned}
&0.20K_{2.00}Mg_{3.89}Fe_{1.42}Al_{2.48}Ti_{0.16}Si_{5.82}O_{20}(OH)_4\\
&\quad + 0.07Na_{0.64}Ca_{0.36}Al_{1.36}Si_{2.64}O_8\\
&\quad + 0.14CaMg_{0.77}Fe_{0.23}Si_2O_6 + 1.04CaCO_3\\
&\quad = 0.42CaMg_{0.72}Fe_{0.28}Si_{2.00}O_6\\
&\quad + 0.11Ca_{2.86}Fe_{0.14}Al_{2.00}Si_{3.00}O_{12} + 0.48CaSiO_3\\
&\quad + 0.60MgO + 0.19FeO + 0.38AlO_{3/2}\\
&\quad + 0.03TiO_2 + 0.02NaO_{1/2} + 0.41KO_{1/2}\\
&\quad + 0.41H_2O + 1.04CO_2
\end{aligned}$$

Appendix S1 lists all the equations necessary to describe the model. The simultaneous equations can be solved for the given ratios of phenomenological coefficients as parameters using MATLAB mathematical software. Figure 8(a) shows an example of an exchange cycle that describes the reaction at each contact and the corresponding fluxes of components across each layer. The diopside zone grows in both directions, while the garnet and wollastonite zones grow towards the marble. As discussed in the *Petrography* section, calcite is preserved in part of the diopside zone, indicating the growth of the diopside zone in both directions. The model is therefore consistent with field observations. CaO is produced at the marble-wollastonite zone boundary, and diffuses down the chemical potential gradient towards the MB before being consumed at the MB-diopside zone boundary. MgO, FeO, $AlO_{3/2}$ and SiO_2 are produced at the MB-diopside zone boundary and diffuse towards the marble.

In some cases, certain values of parameters produce physically unrealistic solutions. Figure 8(b) shows such an example. Both diopside and garnet are produced at the diopside–garnet zone boundary in this case, which is unrealistic. The stability field of the specific zonal sequence can be delineated in the *L*-ratio diagram (Fig. 9). The *L*-ratio field is divided into several regions on the basis of two kinds of boundaries. One is the null production line of the product mineral at the zone boundary, whereas the other is the mass balance line of the open component at the outermost boundaries, where the amount of the component produced or consumed should balance the influx or efflux of the component beyond

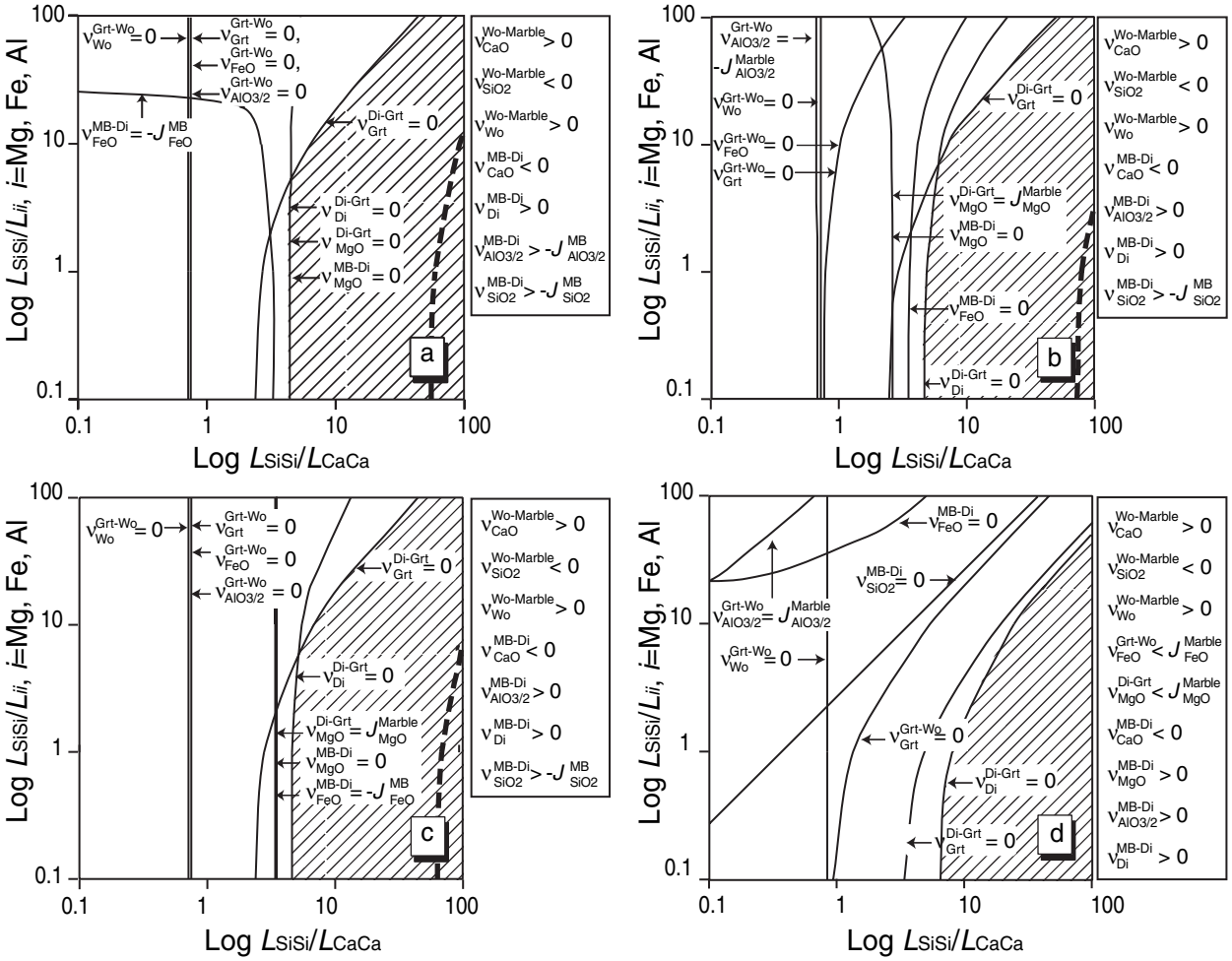

Fig. 9. Stability relationships of possible zonal sequences in a logarithmic scale L-ratio diagram, as obtained from the steady-diffusion model in an open system (Ashworth & Birdi, 1990). Hatched area indicates the stability field of the zonal sequence. The dotted line indicates the L-ratios that yield the amount of diopside consistent with observational data. Blank area shows the fields in which the reaction zone is unstable. Combinations of closure components are (a) CaO and MgO, (b) CaO and FeO, (c) CaO and $AlO_{3/2}$, and (d) CaO and SiO_2.

the boundary. In the case that the amount of a component is insufficient to produce a product mineral at the outermost boundary, the influx of the component from the exterior should compensate for the shortage. If the influx is insufficient to compensate for this shortage, the zonal sequence is unstable. Thus the stability field of a specific zonal sequence is bounded by these two kinds of lines.

Although there are theoretically 16 boundary lines [5 (number of component) × 2 (number of outermost boundary) + 3 (number of product phase) × 2 (number of the boundary of each zone) = 16], only a limited number of lines appear in L-ratio diagrams (Fig. 9). The conditions listed in the boxes in Fig. 9 are always satisfied in the range of L-ratios of the diagrams, and are therefore irrelevant to the stability of the zonal sequence. To examine the stability of the zonal sequence, calculations were made for L-ratios ranging from 0.1 to 100. Figure 9(a–d) shows the results for the four cases of closure components discussed above.

In the calculations, we set $L_{SiSi}/L_{MgMg} = L_{SiSi}/L_{FeFe} = L_{SiSi}/L_{AlAl}$. These ratios will have little effect on the stability of the zonal sequence, as L_{SiSi}/L_{MgMg} concerns only the diopside zone, L_{SiSi}/L_{FeFe} the diopside and garnet zones, and L_{SiSi}/L_{AlAl} the garnet zone. The stability field of the zonal sequence is represented by the hatched area in Fig. 9. In all four cases, the stability field occurs at a relatively large magnitude of L_{SiSi}/L_{CaCa}. The dotted lines represent L-ratios that provide the measured amounts of diopside produced at the MB-diopside and diopside-garnet zone boundaries. These amounts were estimated by measuring the thickness between the initial boundary currently preserved within the diopside zone and the outer boundaries of the diopside zone. In cases 1, 2 and 3 (Fig. 9a, b and c respectively), the values of L_{SiSi}/L_{CaCa} that yield a result consistent with measured values are larger than 56.2, while no value of L_{SiSi}/L_{CaCa} yields a consistent result for case 4 (Fig. 9d).

Results of the Johnson & Carlson (1990) model

The characteristic feature of the Johnson & Carlson (1990) model resides in the boundary-flux equations. The boundary fluxes are estimated by a mass-balance calculation to reproduce product phase ratios, ensuring that the reactant phase ratios in the MB are held constant. As in the previous section, the potential open-system components are SiO_2, MgO, FeO and $AlO_{3/2}$. Four possible choices of closure conditions are able to reproduce the product phase ratios:

Case 1. MgO and CaO are closure components. The boundary fluxes of MgO, FeO and $AlO_{3/2}$ can be estimated as:

$$J_{FeO}^{MB} = 0.0256,\ J_{AlO_{3/2}}^{MB} = 0.0180 \text{ and } J_{SiO_2}^{MB} = 1.0892.$$

Case 2. FeO and CaO are closure components. The boundary fluxes of MgO, $AlO_{3/2}$ and SiO_2 can be estimated as:

$$J_{MgO}^{Marble} = 0.0718,\ J_{AlO_{3/2}}^{Marble} = 0.0296 \text{ and } J_{SiO_2}^{MB} = 0.9589.$$

Case 3. $AlO_{3/2}$ and CaO are closure components. The boundary fluxes of MgO, FeO and SiO_2 can be estimated as:

$$J_{MgO}^{Marble} = 0.0272,\ J_{FeO}^{MB} = 0.0159 \text{ and } J_{SiO_2}^{MB} = 1.0399.$$

Case 4. SiO_2 and CaO are closure components. The boundary fluxes of MgO, FeO and $AlO_{3/2}$ can be estimated as:

$$J_{MgO}^{Marble} = 0.6002,\ J_{FeO}^{Marble} = 0.1885 \text{ and } J_{AlO_{3/2}}^{Marble} = 0.3795.$$

The overall reactions in cases 1–4 are equivalent to those in the Ashworth & Birdi (1990) model described above.

The open-system model of Johnson & Carlson (1990) was applied to each of the four cases; the equations in each case are listed in Appendix S2. Figure 10(a–d) shows the stability region of the zonal sequence in each case in terms of L_{SiSi}/L_{CaCa} and L_{SiSi}/L_{ii} (i = Mg, Fe, Al). The results for all cases are very similar to those of the Ashworth & Birdi (1990) model. The zonal sequence is stable in the hatched area shown in Fig. 10. For cases 1, 2 and 3 (Fig. 10a, b and c respectively), values of L_{SiSi}/L_{CaCa} greater than 56.2 provide results that are consistent with the observed zonal sequence within the reaction zone. No consistent result can be achieved for case 4. Although our model cannot predict which of the three combinations of open components (cases 1–3) is most likely, the occurrence of a composite vein described earlier provides some insight into this problem. As the composite vein is derived from the reaction zone and is composed of garnet, plagioclase and wollastonite, MgO has not be supplied from the reaction zone for the formation of the composite vein. Thus we conclude that case 1 (CaO and MgO as closure components) is most suitable for describing the formation of the reaction zone.

DISCUSSION

In terms of this study, the results of the Ashworth & Birdi (1990) and Johnson & Carlson (1990) open-system models are almost identical; this result indicates the consistency of the two models. *L*-ratio diagrams show several instability fields (blank fields in Figs 9 & 10) for the zonal sequence. We cannot predict from the model the kind of zonal sequence that is stable in the instability fields, as all product zones are monomineralic. This is an intrinsic feature of the steady-diffusion model applied to monomineralic reaction zones. Another characteristic feature of monomineralic reaction zones is that the stability region in *L*-ratio diagrams is dependent on which of the zones grow in both directions.

Care should be taken, however, in applying steady-diffusion models to this problem, as the results are sensitive to the choice of closure components and estimates of boundary fluxes. As shown by Ashworth & Birdi (1990), the isocon analysis provides a powerful tool to determine the closure components in certain cases. In the present study, isocon analysis was unable to determine the closure components, and we were forced to use an alternative approach that considered the ability of different combinations of open components to reproduce product phase ratios. As for boundary fluxes, the solution is sensitive to phase ratios, and the exact determination of phase ratios may be difficult in the case of a zone with irregular boundaries. In our case, the diopside and garnet zones have planar boundaries, but the wollastonite zone has an irregularly curved contact with the adjacent marble. Although the mean width of the wollastonite zone was used in the calculations, some errors in the calculated phase ratios are inevitable. The stability of the zonal sequence, however, will not be seriously influenced by the errors in phase ratios; rather, it will be strongly influenced by the choice of closure components, as demonstrated above.

Mineral assemblages that are in equilibrium with fluids during metamorphism can be used to clarify the nature of the fluid (e.g. Rumble *et al*., 1982; Nishiyama, 1990; Baumgartner & Ferry, 1991; Dipple & Ferry, 1992; Ferry, 1994, 1995; Ferry *et al*., 2001). This study assumes that the intergranular fluid is a CO_2–H_2O binary fluid, as graphite is absent. The overall reaction produces a fluid with $X_{CO_2} = 0.94$ when CaO and MgO are closure components. In contrast, the occurrence of wollastonite suggests a more H_2O-rich fluid, because wollastonite is stable only at X_{CO_2} lower than 0.49 at 700 °C and 300 MPa (Berman, 1988; Mader & Berman, 1991). This provides evidence of the infiltration of a reactive H_2O-rich fluid driving a metamorphic decarbonation reaction. The fluid flow may have occurred parallel to the MB–marble contact and caused significant mass transport perpendicular to the diffusion direction (Fig. 8). The selection of CaO and MgO as closure components is consistent with

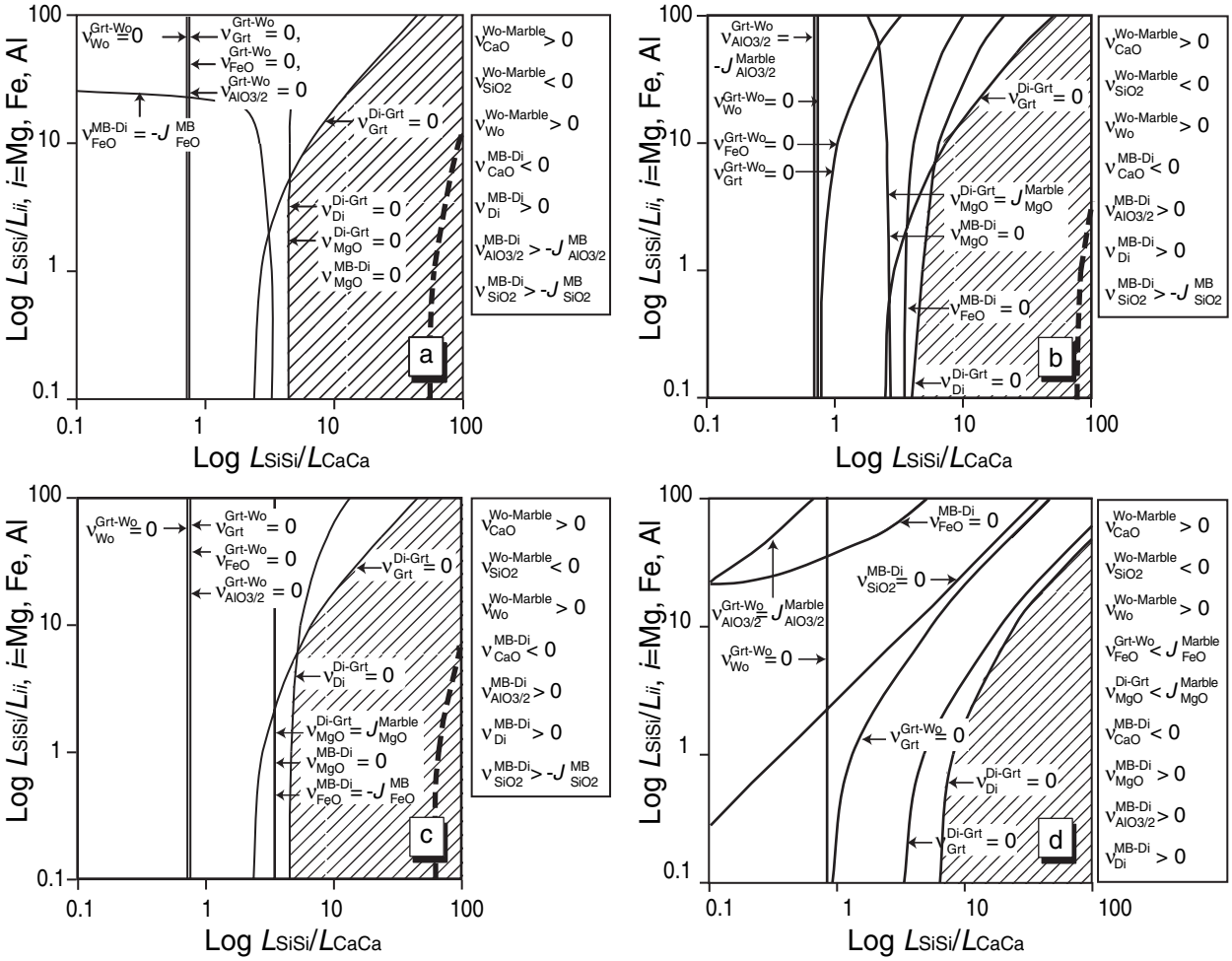

Fig. 10. Stability relationships of possible zonal sequences in logarithmic scale *L*-ratio diagrams, as obtained by the steady-diffusion model in an open system (Johnson & Carlson, 1990). Hatched area indicates the stability field of the zonal sequence. The dotted line indicates the *L*-ratios that yield the amount of diopside production consistent with observational data. Blank area shows the field in which the reaction zone is unstable. Combinations of closure components are: (a) CaO and MgO, (b) CaO and FeO, (c) CaO and $AlO_{3/2}$, and (d) CaO and SiO_2.

the advection of an H_2O-rich fluid, as indicated by the occurrence of a composite garnet + plagioclase + wollastonite vein for which the components (FeO, SiO_2 and $AlO_{3/2}$) may have been transported by the fluid, except for CaO, which was supplied from the marble wall rock.

CONCLUSIONS

In this study, two kinds of steady-diffusion models were applied: Ashworth & Birdi (1990) and Johnson & Carlson (1990), to a reaction zone between a metamorphosed basic dyke and marble. From the dyke to the marble, the reaction zone consists of a diopside zone, a garnet zone, and a wollastonite zone, in that order. The two models provide essentially the same results in terms of the stability region of the zonal sequence in *L*-ratio diagrams. We conclude that the two versions of open-system models are consistent with each other, although calculation procedures are somewhat different.

Certain features that are intrinsic to monomineralic reaction zones are depicted with respect to the stability of the zonal sequence in *L*-ratio diagrams. The stability regions of the zonal sequence are bounded by null production lines of one of the product minerals with outer regions where no possible zonal sequence can be predicted.

The infiltration of H_2O-rich fluid is inferred from wollastonite stability; this event caused a decarbonation reaction and vein formation, as indicated by the occurrence of a garnet + plagioclase + wollastonite composite vein.

ACKNOWLEDGEMENTS

We greatly appreciate H. Isobe for his help in EPMA analyses and for discussions related to this research.

Critical and constructive comments from J. M. Ferry and W. D. Carlson and editorial work by M. Brown are gratefully acknowledged. Thanks are also due to S. Nohda, M. Aniya, K. Miyazaki, T. Miyamoto, H. Mashima and K. Maki for discussions and support in conducting experiments. This work was financially supported by Grant-in-Aid for Scientific Research A (no. 17204045 to T. Nishiyama) and Grant-in-Aid for Young Scientists B (No. 16740303 to Y. Mori), both from the Ministry of Education, Science, Sports and Culture, Japanese Government.

REFERENCES

Ashworth, J. R. & Birdi, J. J., 1990. Diffusion modelling of coronas around olivine in an open system. *Geochimica et Cosmochimica Acta*, **54,** 2389–2401.

Ashworth, J. R. & Sheplev, V. S., 1997. Diffusion modelling of metamorphic layered coronas with stability criterion and consideration of affinity. *Geochimica et Cosmochimica Acta*, **61,** 3671–3689.

Ashworth, J. R., Sheplev, V. S., Bryxina, N. A., Kolobov, V. Yu. & Reverdatto, V. V., 1998. Diffusion-controlled corona reaction and overstepping of equilibrium in a garnet granulite, Yenisey Ridge, Siberia. *Journal of Metamorphic Geology*, **16,** 231–246.

Attoh, K., 1998. Models for orthopyroxene-plagioclase and other corona reactions in metanorites, Dahomeyide orogen, West Africa. *Journal of Metamorphic Geology*, **16,** 345–362.

Baumgartner, L. P. & Ferry, J. M., 1991. A model for coupled fluid-flow and mixed-volatile mineral reactions with applications to regional metamorphism. *Contributions to Mineralogy and Petrology*, **106,** 273–285.

Baumgartner, L. P. & Olsen, S. N., 1995. A least-squares approach to mass transport calculations using the isocon method. *Economic Geology*, **90,** 1261–1270.

Berman, R. G., 1988. Internally-consistent thermodynamic data for minerals in the system Na_2O-K_2O-CaO-MgO-FeO-Fe_2O_3-Al_2O_3-SiO_2-TiO_2-H_2O-CO_2. *Journal of Petrology*, **29,** 445–522.

Brady, J. B., 1977. Metasomatic zones in metamorphic rocks. *Geochimica et Cosmochimica Acta*, **41,** 113–126.

Dipple, G. M. & Ferry, J. M., 1992. Metasomatism and fluid flow in ductile fault zones. *Contributions to Mineralogy and Petrology*, **112,** 149–164.

Ferry, J. M., 1994. Overview of the petrologic record of fluid flow during regional metamorphism in Northern New England. *American Journal of Science*, **294,** 905–988.

Ferry, J. M., 1995. Fluid flow during contact metamorphism of ophicarbonate rocks in the Bergell aureole, Val Malenco, Italian Alps. *Journal of Petrology*, **36,** 1039–1053.

Ferry, J. M., Wing, B. A. & Rumble, D., 2001. Formation of wollastonite by chemically reactive fluid flow during contact metamorphism, Mt. Morrison Pendant, Sierra Nevada, California, USA. *Journal of Petrology*, **42,** 1705–1728.

Fisher, G. W., 1973. Non-equilibrium thermodynamics as a model for diffusion controlled metamorphic processes. *American Journal of Science*, **273,** 897–924.

Fisher, G. W., 1978. Rate laws in metamorphism. *Geochimica et Cosmochimica Acta*, **42,** 1035–1050.

Foster, C. T., 1981. A thermodynamic model of mineral segregations in the lower sillimanite zone near Rangeley, Maine. *American Mineralogist*, **66,** 260–277.

Foster, C. T., 1983. Thermodynamic models of biotite pseudomorphs after staurolite. *American Mineralogist*, **68,** 389–397.

Foster, C. T., 1986. Thermodynamic models of reactions involving garnet in a sillimanite/staurolite schist. *Mineralogical Magazine*, **50,** 427–439.

Fukuyama, M., Urata, K. & Nishiyama, T., 2004. Geology and petrology of the Hirao Limestone and the Tagawa metamorphic rocks-with special reference to the contact metamorphism by Cretaceous granodiorite. *Journal of Mineralogical and Petrological Science*, **99,** 25–41.

Goto, A., Horie, T., Ohba, T. & Fujimaki, H., 2002. XRF analysis of major and trace elements for wide compositional ranges from silicate rocks to carbonate rocks using low dilution glass beads. *Japanese Magazine of Mineralogical and Petrological Science*, **31,** 162–173.

Grant, J. A., 1977. Crystallographic projection of chemical potential relationships as an aid in the interpretation of metasomatic zoning. *American Mineralogist*, **62,** 1012–1017.

Grant, J. A., 1986. The isocon diagram – a simple solution to Gresens' equation for metasomatic alteration. *Economic Geology*, **81,** 1976–1982.

Grant, S. M., 1988. Diffusion models for corona formation in metagabbros from the western Grenville province, Canada. *Contributions to Mineralogy and Petrology*, **98,** 49–63.

Gresens, R. L., 1967. Composition-volume relationships of metasomatism. *Chemical Geology*, **2,** 47–65.

de Groot, S. R. & Mazur, P., 1984. *Non-equilibrium Thermodynamics*. Dover Publications, New York.

Joesten, R., 1977. Evolution of mineral assemblage zoning in diffusion metasomatism. *Geochimica et Cosmochimica Acta*, **41,** 649–670.

Joesten, R., 1986a. The role of magmatic reaction, diffusion and annealing in the evolusion of coronitic microstructure in troctolitic gabbro from Risor, Norway. *Mineralogical Magazine*, **50,** 441–469.

Joesten, R., 1986b. The role of magmatic reaction, diffusion and annealing in the evolution of coronitic microstructure in troctolitic gabbro from Risor, Norway: reply. *Mineralogical Magazine*, **50,** 474–479.

Joesten, R., 1991. Local equilibrium in metasomatic processes revisited: diffusion-controlled growth of chert nodule reaction rims in dolomite. *American Mineralogist*, **76,** 743–755.

Joesten, R. & Fisher, G., 1988. Kinetics of diffusion-controlled mineral growth in the Christmas Mountains (Texas) contact aureole. *Geological Society of American bulletin*, **100,** 714–732.

Johnson, C. D. & Carlson, W. D., 1990. The origin of olivine-plagioclase coronas in metagabbros from the Adirondack Mountains, New York. *Journal of Metamorphic Geology*, **8,** 697–717.

Katchalsky, A. & Curran, P. F., 1965. *Nonequilibrium Thermodynamics in Biophysics*. Harvard University Press, Cambridge.

Kawano, Y. & Ueda, Y., 1966. K-A dating on the igneous rocks in Japan (IV)-granitic rocks in northeastern Japan-. *Journal of Mineralogy, Petrology and Economic Geology*, **56,** 191–211.

Korzhinskii, D. S., 1959. *Physicochemical Basis of the Analysis of the Paragenesis of Minerals*. Consultants Bureau, New York.

Kretz, R., 1983. Symbols for rock-forming minerals. *American Mineralogist*, **68,** 277–279.

Mader, U. K. & Berman, R. G., 1991. An equation of state for carbon dioxide to high pressure and temperature. *American Mineralogist*, **76,** 1547–1559.

Mori, Y. & Mashima, H., 2005. X-ray fluorescence analysis of major and trace elements in silicate rocks using 1:5 dilution glass beads. *The Bulletin of the Kitakyushu Museum of Natural History and Human History*, **3,** 1–12.

Nishimura, Y., 1998. Geotectonic subdivision and areal extent of the Sangun belt, Inner Zone of Southwest Japan. *Journal of Metamorphic Geology*, **16,** 129–140.

Nishiyama, T., 1983. Steady diffusion model for olivine-plagioclase corona growth. *Geochemica et Cosmochimica Acta*, **47,** 283–294.

Nishiyama, T., 1989. Kinetics of hydrofracturing and metamorphic veining. *Geology*, **17,** 1068–1071.

Nishiyama, T., 1990. CO_2-metasomatism of a metabasite block in a serpentine melange from the Nishisonogi metamorphic

rocks, southwest Japan. *Contributions to Mineralogy and Petrology*, **104,** 35–46.
Prigogine, I., 1967. *Introduction to Thermodynamics of Irreversible Processes*, 3rd edn. Interscience, New York.
Rumble, D., Ferry, J. M., Hoering, T. G. & Boucot, A. J., 1982. Fluid flow during metamorphism at the Beaver Brook fossil locality, New Hampshire. *American Journal of Science*, **282,** 886–919.
Thompson, J. B., 1959. Local equilibrium in metasomatic processes. In: *Researches in Geochemistry* (ed. Abelson, P. H.), pp. 427–457. John Wiley, New York.
Thompson, J. B., 1982. Reaction space: an algebraic and geometric approach. In: *Characterization of Metamorphism through Mineral Equilibria, Reviews in Mineralogy 10* (ed. Ferry, J. M.), pp. 33–52. Mineralogical Society of America, Washington, DC.

Received 24 December 2004; revision accepted 9 December 2005.

SUPPLEMENTARY MATERIAL

The following supplementary material is available from http://www.blackwell-synergy.com:

Appendix S1. Ashworth & Birdi (1990) model.
Appendix S2. Johnson & Carlson (1990) model.